Augmented Collisional Ionization in the VUV regime; a theoretical study

Nicolas Bigaouette* and Lora Ramunno†
Department of Physics, University of Ottawa, 150 Louis Pasteur, Ottawa ON, K1N 6N5, Canada

Edward Ackad‡
Department of Physics, Southern Illinois University Edwardsville,
State Route 157 Edwardsville, IL 62026, United States
(Dated: August 22, 2013)

We revisit a major 2002 experiment at FLASH-DESY FEL facilities on Xenon clusters interacting with VUV (98 nm, 12.65 eV) 100 fs laser pulses. Previously thought to have an intensity of 2×10^{13} W/cm^2 it was later re-calibrated in 2010 to 8×10^{12} W/cm^2, less than half the initial value. In light of this new intensity, we revisit this experiment in the VUV regime by applying our Augmented Collisional Ionization (ACI) model. Included also is single photon ionization, impact ionization and (in some simulations) recombination. At this wavelength and intensity, tunnel and multi-photon ionization are negligible and are thus not included. We found that ACI increases both the maximum charge state seen and the most abundant one, both by two states higher. ACI was required to match the experimental data. A deeper potential depth as used in other studies revealed a large influence on charge state spectrum.

I. INTRODUCTION

The advance of Free Electrons Lasers (FEL) around the world gave access to unprecedented intensity at wide range of wavelengths, including from the VUV to X-ray. Recent experiments have studied the interaction of such laser pulses with clusters of atoms. These clusters are nanoscopic objects at solid density. Additionally, their finite size makes them easier to study, both theoretically and experimentally.

Many studies of the interaction of laser-matter have been done at wavelengths ranging from the IR to X-ray regimes. Experiments in 2002 by Wabnitz *et al.*[1] at FLASH-DESY FEL facilities on clusters of Xenon and VUV radiation saw surprisingly high charge states (Xe^{8+}) using 98 nm (12.7 eV) pulses at an intensity of (what was thought at the time) 7×10^{13} and 2×10^{13} W/cm^2.

The mechanisms known at that time could not explain the high charge states seen in the experiments[2] and as such, more theoretical work was required.

Based on the original 2002 intensity calibration, three major models have emerged to explain the high ionization levels. First, the lowering of the potential barrier was suggested for photo-ionization [3–6] where a neighbouring ion lowers the barrier, making the absorption of a single photon by the electron energetically possible.

Second, Santra and Green suggested using atomic potential instead of the Coulomb potential. They used a simple screening potential [7] and later a more realistic one [8] based on a Hartree-Fock-Slater code written by F. Herman and S. Skillman [9] and saw 30 times more VUV photons absorbed by a cluster environment compared with using a simple Coulomb potential. Furthermore, charge states up to Xe^{6+} for Xe_{1500} clusters were obtained with simulations using the atomic potentials.

Due to the high density of particles in a cluster environment, Jungreuthmayer *et al.*[2] identified an additional mechanism called "Multi-Body Recombination" (MBR) heating. Due to the high density and highly collisional nature of the strongly coupled plasma created in clusters by VUV laser pulses, electrons can cool down through collisions in the ion's potential well and recombine to a highly excited state. This newly recombined electron can then reabsorb a new photon from the laser, effectively increasing the system's energy absorption from the laser. Using a classical approach to the particles' dynamics, they observed high charge states up to 7+ for their highest intensity (7×10^{13} W/cm^2).

In 2010, the intensity of the DESY-FEL pulses[1] was revised by Bostedt *et al.*[10] to a lower value of 8×10^{12} W/cm^2 instead of the previously thought 2×10^{13} W/cm^2. At this reduced intensity the known mechanisms will have a reduced effect too. This increases the need for more theoretical work. In light of these new parameters, we propose revisiting this 2002 experiment.

Lastly, our group suggested that atomic excited states might be extremely important for understanding the high charge states seen in cluster experiments. While our previous work was for Argon in the XUV (32.8 nm, 37.8 eV) regime[11, 12] and Xenon in soft X-rays (13.7 nm, 90.5 eV) regime[13], the process of "Augmented Collisional Ionization" (ACI) may play an important role in other regimes as well.

In the first part of this paper, we will describe our classical approach to the clusters' dynamics followed by the different ionization processes which are treated quantum mechanically. Results are then presented by first showing the influence ACI has on the maximum charge states seen in simulations. Then, the cluster size influence is

* nbigaouette@gmail.com
† lramunno@uottawa.ca
‡ eackad@siue.edu

studied and compared to experiments by averaging over the spacial distribution of the laser pulse. Last, we investigate the influence of the potential depth used in our simulations on the maximum charge state seen.

II. MODEL

Clusters are nanoscopic systems and as such are hard to model using statistical approaches which often assume infinite systems. Our model thus tracks every particle present using a classical molecular dynamics (MD) code. Such MD codes are excellent tools for the simulation of a low number of particles since no approximation is used (apart from the classical instantaneous electrostatic interactions). Unfortunately, the N-body problem has no analytic solutions and is chaotic, requiring large amount of data for valid statistics. Furthermore, the MD interaction calculation has an $O(N^2)$ scaling which renders simulations of more than tens of thousands of particles using long range interactions virtually impossible. Approximation to the N-body problem are possible; hierarchical tree code [14] and fast-multipole methods [15] can reduce the burden to an $O(N \log(N))$ problem.

These algorithms have overheads which makes them slower for a low number of particles. They can also introduce some errors in the force and potential calculations. While these errors are not significant for the dynamics aspect of the simulation, they can influence the calculated rates of quantum transitions used throughout the code.

Instead of using tree-based algorithms, we decided to port the classical dynamics aspect of the simulation to the OpenCL framework. This allows us to accelerate calculation on general-purpose graphical processing units (GP-GPU) similarly to Nvidia's CUDA. Contrary to the later, OpenCL is not bound to specific hardware vendor or even accelerator devices. For example, multi-core CPUs can also be used to accelerate calculation, making the code portable to many different architectures. It is not uncommon to see speedups of the order of 100 using GPGPUs. In our case, a speedup between 40 and 80 was seen when using an Nvidia GTX 580 GPU and our group's computer cluster with 20 Nvidia Tesla C2075 was used for the present work.

The Coulomb interaction between particles is cut at small distances to mitigate numerical errors due to the singularity. Particles are treated as gaussian charge densities where the potential is given by (in atomic units):

$$\phi(r) = \frac{Z}{r} \mathrm{erf}\left\{ \frac{r}{\sigma\sqrt{2}} \right\} \tag{1}$$

with erf{} the error function, Z the charge state of the particle and σ the width of the charge density given by:

$$\sigma = \frac{Z}{D}\sqrt{\frac{2}{\pi}} \tag{2}$$

The maximum depth of the potential of a $Z = 1$ ion is given by the parameter D. Note that at large distances ($r >> \sigma$), this smoothed potential converge to the Coulomb potential.

Initially, the simulated cluster is neutral. As time passes, the laser's energy, modelled as both an oscillating electric field with a carrier envelope and a flux of photons, is absorbed. Electrons are created in the code and their movement, as the new ions', is calculated classically. Many mechanisms, described next, play an important role in the energy absorption and diffusion throughout the cluster.

A. Single photon ionization

Since initially the cluster is neutral, the first step to ionization is the absorption of photons. At the studied intensities (10^{12} to 10^{13} W/cm^2) and wavelengths (98 nm, 12.65 eV), field ionization (tunnelling) is negligible, as is multi-photon ionization.

The laser is treated as a photon probability distribution following the intensity profile which is depleted as photons are absorbed. Experimental cross sections for Xenon in the VUV regime were taken from experimental data [16]. These cross-sections are converted to rates and a Monte-Carlo test evaluates the ionization probability.

New electrons then move freely in the cluster environment with an initial energy being the photon's minus the ionization potential (Ip).

Note that a 98 nm (12.65 eV) photon can directly ionize a neutral Xenon (with an Ip of 12.27 eV) but not a Xe^{1+} (with an Ip of 21.4 eV). Single photon ionization can thus not explain the high charge states seen in experiments by itself.

B. Threshold V_p

Many processes are described by using isolated atoms. For example, the semi-empirical Lotz cross-sections for impact ionization assumes the impacting electron comes from infinity where its potential energy is null. However the cluster environment does have an influence on the atomic states which must be taken into account.

We model these interactions as those of an isolated system residing in a constant potential created by the cluster environment. This potential V_p is the contribution of all particles outside the nearest neighbour distance in the pre-ionized cluster.

C. Impact ionization

Once electrons are created in the simulations they will impact atoms, ions and other electrons. While the later is treated as a classical collision, the former can result in the creation of extra electrons through impact ionization.

Impact ionization is implemented using the semi-empirical Lotz cross-sections [17] with parameters taken from [18] for the neutral and [19] for ionized Xenon. The impact parameter b of the impacting electron is calculated through $b = |\mathbf{v} \times \mathbf{r}| / |\mathbf{v}|$ where $\mathbf{v}$ is the impacting electron's velocity vector and $\mathbf{r}$ the vector from the impacting electron to the target. If the impacting parameter lies inside the calculated cross section, ionization takes place.

The impacting electron must have enough kinetic energy to overcome the ionization barrier, which is taken care by having a null cross-section for lower energy impact. Additionally, the ion's threshold is taken to be V_p as explained previously. Instead of using the impacting electron's total energy E in Lotz formula, its total energy with respect to the threshold V_b is used instead. If the electron's effective total energy E' is greater then the Ip and the impact parameter b lies inside the calculated cross-section, the ionization succeeds. A new electron is created in the simulation and energy is removed from the impacting electron.

D. Augmented Collisional Ionization (ACI)

We introduced a novel model [12] which we dubbed "Augmented Collisional Ionization" (ACI) that successfully described the high charge states seen in previous Argon experiments at 32.8 nm [20] and Xenon clusters in soft X-rays (13.7 nm, 90.5 eV) [13, 21]. ACI plays a critical role in the clusters ionization and the subsequent dynamics.

In the ACI model, electrons are created in a two step process. Similarly to impact ionization described above, an electron collides with the atom or ion. In contrast with impact ionization, the final state is not an ion plus two electrons but a single electron and an excited atom or ion. Once excited, an atom or ion can be impact-ionized more easily by a second, lower energy, electron. By using this two steps process, electrons in the low energy tail of the kinetic energy spectrum can also contribute to the cluster ionization. Additionally, more ionization paths are present in the model.

ACI is modeled similarly to impact ionization. Cross sections for the different transitions are taken from a Hartree-Fock implementation of the Cowan code[22]. Due to the finite nature of computers, only the transitions cross-sections of a subset of all infinite number of excited states are calculated. For this work on Xenon clusters, eight excited states ($l < 4$) per charge state are used, for ionization levels up to Xe^{17+}. We emphasize that this a lower bound on the effect of ACI; the inclusion of more excited states would add more ionization channels and potentially increase the effect.

E. Recombination

We include in out model recombination to ground state as described in details in reference [13]. When an electron's total energy with respect to the V_p threshold becomes lower than the (recombination) Ip due to collisions, this electron is recombined with the parent ion and disappear from the simulation. The ion's charge state is updated to reflect the process.

This allows having a potential that is as close as Coulombic as possible (except at really close range where the potential converges to $\phi = ZD$) without having electrons with classical energy below the recombination Ip. Interestingly, it also accelerate the $O(N^2)$ force calculation by reducing the number of particles in the system.

F. Many Body Recombination

MBR is automatically included in a classical MD simulation and is thus included in our results.

An important distinction between MBR and ACI is the direction in which the electronic transition takes place. In the case of ACI, the transition is going "up the energy ladder": a bound electron first in the ground state will receive energy from an impacting electron. Afterwards, the excited atom is ionized more easily by other impacting electrons due to, firstly, the cross-section of the excited state to continuum state being larger than the cross-section from the ground state to continuum. Secondly, the energy required for the excited state to continuum transition is less than that of the ground state to continuum transition and as such more free electrons have a chance to ionize the excited atom. On the other hand, MBR is a transition from the continuum to a highly excited state. While the later is treated purely classically, the former is implemented using cross-sections taken from a Hartree-Fock calculation. The lower excited states used in ACI are distant from each other and must be treated discretely while the higher states in MBR are so dense that their classical treatment does not result in much error. Additionally, while ACI is independent of the laser field and only describes electron-ion collisions, the laser plays an active role in MBR.

III. RESULTS

When irradiated with a 98 nm (12.95 eV) laser pulse, the cluster becomes fully ionized rapidly. This is due to the fact that single photon ionization cross-section is largest (68 Mb) at this longer wavelength for neutral Xenon. Since the photon energy is not sufficient to ionize a Xe^{1+} to a Xe^{2+}, only the first charge state is accessible through single photon ionization. Larger charge states are caused by other mechanisms as is evidenced by experiments with gas targets.

Similarly to reference [2], the Coulomb potential is cut-off at close range to prevent the large field close to the discontinuity to cause numerical heating. Equation (1) is used for the cut-off with $D = 12$ eV. Such a shallow value is used to compare with previous publications where recombination is not present. Even though in a classical simulation an electron orbiting in a Coulomb potential can have a range of energy from zero to minus infinity, fixing the maximum depth of the potential to 12 eV prevents the orbiting electron from having a classical energy less than the recombination energy. Allowing an electron to have an energy below this recombination threshold value would also allow the electron to transfer its energy to other particles, artificially heating the system. This problem is prevented by simply choosing a potential depth D close to the ionization potential of the neutral Xenon.

The small nature of these clusters, the random process of the Monte-Carlo ionization procedures and the chaotic nature of the many-body problem requires acquiring a large sample for valid statistics; for small clusters, 5,000 simulations were run for both ACI disabled and enabled. For larger clusters 100 simulations were performed for both ACI disabled and enabled.

The cluster dynamics after the laser pulse is mainly an expansion; no significant ionization has been observed during that time. As such, simulations were run up to 400 fs which is approximately 150 fs after the end of the laser pulse. We have not seen any major changes when continuing the simulations to longer times.

Cross-sections used in this work were taken from experimental data from reference [16] for single photon ionization. For impact ionization, experimental cross-sections from references [18] and [19] rather than Lotz [17] were used.

A. ACI influence on highest charge state

We first compare the highest charge states seen in both our simulations and the 2002 experiment at DESY. We ran simulations on Xe_{90} clusters to compare with figure 1 of Wabnitz *et al.*. Additionally, the intensity of the 2002 experiment was re-calibrated in 2010[10] from 2×10^{13} to 8×10^{12} W/cm^2, around 40 % of the initial value. We thus ran our simulations at the lower, revised intensity.

Figure 1 shows the resulting charge state spectrum. The left subplot shows data when ACI is not enabled, while the right subplot shows the spectrum when ACI is enabled, with the ratio of excited states in hatched regions.

As we can see, ACI increases by two the maximum charge state from Xe^{3+} to Xe^{5+}. The 2002 experiment showed a clear signal for at least Xe^{4+} for Xe_{80} clusters. We could barely see a Xe^{3+} in our simulations without ACI ($\sim$0.2 %) while a Xe^{4+} is clearly seen when ACI is enabled, similarly to the experimental data.

At the (revised) intensity of 8×10^{12} W/cm^2, the next larger clusters are $Xe_{30,000}$ (revised in 2010 to $Xe_{90,000}$) which are not accessible in our simulations due to computational limitations. Data for $Xe_{1,500}$ was presented in [1] but at the larger intensity of 7.3×10^{13} W/cm^2. If the same re-calibration is applied to this intensity, we can compare with our simulation results of $Xe_{1,000}$ at 1.5×10^{13} W/cm^2 shown on figure 2. When ACI is disabled, the maximum charge state seen is Xe^{5+} but at an insignificant ratio ($\sim$0.01 %) that would be lost in the noise of experimental data. On the contrary, some Xe^{7+} if found when ACI is enabled (with Xe^{6+} being more realistic), an increase of 2. Experimental data shows a maximum of Xe^{8+}.

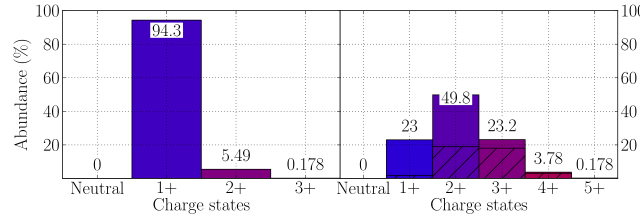

FIG. 1: Charge states spectra of Xe_{90} clusters at $8{\times}10^{12}$ W/cm^2 with ACI disabled (left) and enabled (right)

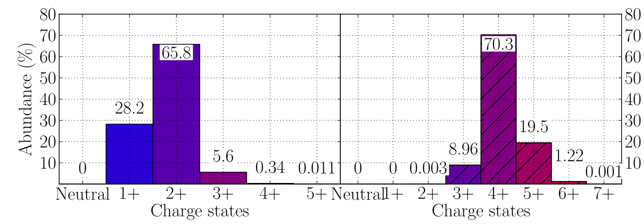

FIG. 2: Charge states spectra of Xe_{1000} clusters at $1.5{\times}10^{13}$ W/cm^2 with ACI disabled (left) and enabled (right)

This is a clear indication that ACI plays a vital role in the dynamics and cannot be ignored when experiments are discussed.

We also measured the number of electrons which are in a Many-Body Recombination (MBR) state. We found that around 18 % of the total number of electrons are in an MBR state, close to the value from reference [2] (around 25 %), an indication that MBR is still important in the description of the dynamics.

B. Laser spacial profile

The previous results can only predict the highest charge state seen. For more precise spectra the spacial profile of the laser must be considered.

We assume here that the density of clusters coming out of the nozzle is constant in space over the whole laser focus. As such, the clusters distributed across the focus' spatial profile will sample a different laser intensity de-

Distance to focus	Normalized height	Intensity ($\times 10^{12}$ W/cm^2)
0	1	8.000
$\sqrt{-2\sigma^2 \ln\left(\frac{1+e^{-1/2}}{2}\right)}$	$\frac{1+e^{-1/2}}{2}$	6.424
σ	$e^{-1/2}$	4.852
$\sigma\sqrt{2\ln(2)}$	1/2	4.000
$\sqrt{2}\sigma$	e^{-1}	2.943
2σ	e^{-2}	1.083

TABLE I: Intensity of laser pulse at different distances of the focus assuming a gaussian spatial profile with a standard deviation σ.

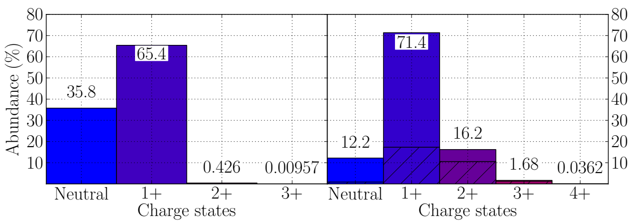

FIG. 3: Charge states spectra of Xe_{90} using intensities of table I. ACI disabled (left) and enabled (right)

pending on their distance from the focus' centre. This is taken into account by running many different simulations at different intensities. Each intensity is then weighted accordingly to represent the different location in the laser's focus two dimensional cross section profile.

The peak intensity of the experiment being 8×10^{12} W/cm^2, we chose the values for the simulations shown on table I. Considering a focus diameter (FWHM) of $\tau = 20\mu$m we have $\sigma = \tau\left(2\sqrt{2\ln(2)}\right)^{-1} = 11.77\mu$m.

We study the influence of the cluster size on the charge states spectra similarly as figure 1 from Wabnitz *et al.* (or figure 2 from reference Bostedt *et al.*) but due to computational resources limits, the largest clusters simulated were $Xe_{5,083}$.

Figure 3 shows the charge state distribution for Xe_{90} clusters and figures 4, 5 and 6 show the distribution of icosahedral clusters with their 7th, 8th and 11th closed shells ($Xe_{1,415}$, $Xe_{2,057}$ and $Xe_{5,083}$, respectively). All icosahedral configurations were relaxed using a Lennard-Jones potential for neutral xenon.

Each figure shows the results of our simulations using the same parameters as the DESY-FEL experiment [1, 10] and all intensities shown on table I. For the smallest cluster size (Xe_{90} on figure 3), ACI increases the highest charge states by one, from Xe^{3+} to Xe^{4+}. For the next larger clusters ($Xe_{1,415}$), ACI increases the highest charge state observed by two, from Xe^{3+} to Xe^{5+}. Finally, the two largest cluster sizes ($Xe_{2,057}$ and $Xe_{5,083}$) see their largest charge state increase from Xe^{4+} to Xe^{5+} when ACI is enabled.

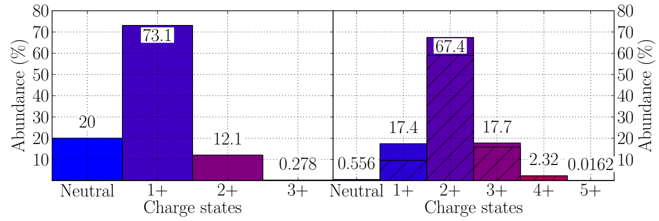

FIG. 4: Charge states spectra of $Xe_{1,415}$ using intensities of table I. ACI disabled (left) and enabled (right)

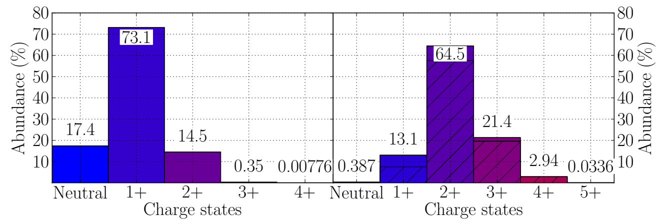

FIG. 5: Charge states spectra of $Xe_{2,057}$ using intensities of table I. ACI disabled (left) and enabled (right)

Additionally, the most abundant charge state is shifted from Xe^{1+} to Xe^{2+} when ACI is enabled for large clusters, while staying at Xe^{1+} for the smallest (Xe_{90}) clusters.

Figures 3, 4, 5 and 6 are in good agreement with the DESY experiment [1, 10]: the dominant charge states seen was Xe^{2+} for the largest clusters ($Xe_{90,000}$) while for the smallest (Xe_{70}) the Xe^{1+} ion was dominant.

We can see that figures 4, 5 and 6 are quite similar except from the fact that the distribution is shifting to larger values as the cluster size increases. Without ACI, the populations of Xe^{3+} goes from 0.28 to 0.35 to 0.59 percent as the cluster size increase from $Xe_{1,415}$ to $Xe_{2,057}$ to $Xe_{5,083}$. The Xe^{3+} population doubles between the $Xe_{1,415}$ and $Xe_{5,083}$ clusters.

Even though $Xe_{5,083}$ clusters are less than four times larger than $Xe_{1,415}$, they have 4 more closed shells. The doubling of the Xe^{3+} is likely caused by the number of ions on the cluster surface increasing more slowly than the number of ions in the cluster volume. For example,

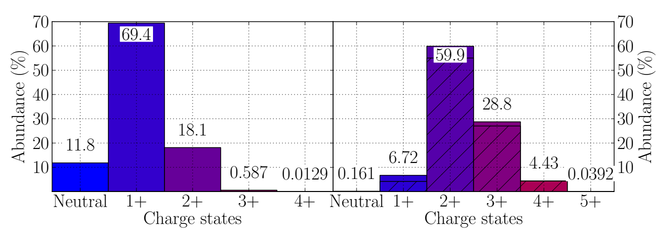

FIG. 6: Charge states spectra of $Xe_{5,083}$ using intensities of table I. ACI disabled (left) and enabled (right)

the $Xe_{1,415}$ clusters have 35 % of atoms inside their volume, while this proportion drops to 24 % for $Xe_{5,083}$. Since we have seen that the higher charge states reside on the cluster boundaries, as reported in [11], we expect to see a slower increase of the yield of the highest charge states compared to the cluster size increase.

C. Effect of deeper potentials

The potential depth of 12 eV used for the cutoff is arbitrary. In reality, electrons will feel a complete potential. However, due to the classical nature of our model, using an infinite potential (for example Coulombic) would allow electrons to fall too deep, causing un-physical heating of the other electrons due to energy conservation.

As suggested in previous studies[7, 8] the shape and depth of the ion potential does have an influence on the dynamics. Using a deeper potentials will allow a larger scattering angle required for heating of the cluster through IBH. To explore this avenue, we now need to used recombination as described in our previous work[13]. This allows using a deeper potential while preventing un-physical events.

As the potential gets deeper, the field close to the ion increases and a smaller time step must be used. For such deep potentials, the limit on the floating point precision of the computer becomes apparent and decreasing the time step used does not decrease the error anymore. Additionally, simulations using a time step smaller than 0.05 attosecond become intractable as the simulations time increase to many months.

We have thus settled on a time step of 0.15 as which minimizes the calculation error while still providing reasonable simulation duration. We compared the following results with a time step of 0.1 as and found only negligible differences in the charge states distribution.

Additionally, since recombination will change the charge state distribution even after the laser has passed by redistributing energy throughout the cluster, simulations must be run for a longer time. In this case, simulations went up to 1 ps where the cluster is fully exploded.

We find that the depth of the potential does have an influence on the cluster dynamics. We note that no spacial averaging (as in the previous subsection) was performed here. As the potential gets deeper, a smaller time step must be used which slows down simulations significantly. We thus only compare the highest charge states in the spectra.

Figures 7a, 7b and 7c show the results for Xe_{80} clusters under a 8×10^{12} W/cm^2 laser pulse for a potential depth D of 12 eV (0.441 Eh), 27.2 eV (1 Eh) and 81.63 eV (3 Eh) – see equation (2). Similarly to other figures, the left hand part has ACI disabled while the right hand part of the figures has ACI enabled, with the ratio of excited states in hatched regions. We clearly see an increase in both the maximum and dominant charge state seen as the potential depth gets deeper. While the shallow potential depth of 12 eV gives interesting results, we see that a deeper potential is required to obtain higher charge states. We also see that at $D = 3$ Eh, the distribution is similar to the one at $D = 1$ Eh, an indication of the saturation of the energy absorption. It is thus not necessary to go deeper than 1 Eh to extract the full dynamic of the cluster.

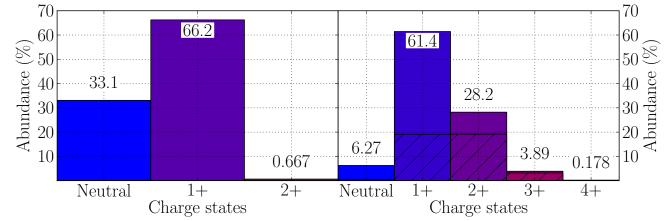

(a) $D = 12$ eV (0.441 Eh)

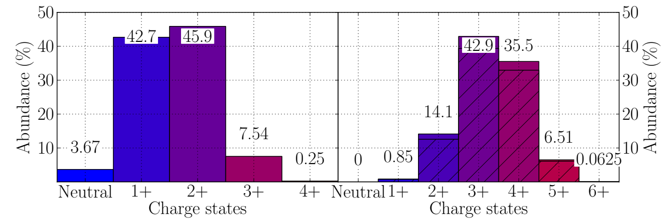

(b) $D = 27.2$ eV (1 Eh)

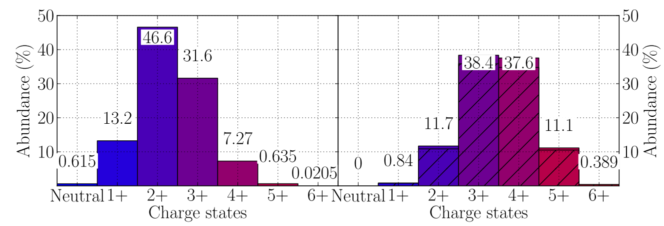

(c) $D = 81.63$ eV (3 Eh)

FIG. 7: Charge state spectra after 1 ps of Xe_{80} using an intensity of 8×10^{12} W/cm^2 and different potential depth D (see equation (2))

These results can be explained by the increase in IBH due to the electrons being able to sample a deeper ion potential. Though the potential used here is Coulombic, it is similar in idea to what Santra and Greene suggested[7, 8] where the deeper parts of the potential do contribute significantly.

We do note that when ACI is not present the spectra of figures 7 show a large variation depending on the potential depth D. This is due to the small size of Xe_{80} clusters where a single ionization event has a large relative weight on the spectrum shape. Nevertheless, it seems ACI does stabilize this variation by increasing the ionization levels.

Note that due to the smaller time step used in this section not as many runs could be performed as was done in the previous section; 60 runs were used to generate every charge state spectrum shown on figures 7

IV. CONCLUSION

In summary, many refinements were made on previous models. For example, a smoother shape of the close range potential was used, removing the need for extremely small time steps to keep numerical heating under control. Additionally, the classical dynamics part of the code was re-written to run on GP-GPU using OpenCL for a 40 to 80 times speed increase. This allowed us to increase the number of simulations we ran and thus their statistical significance or to push the simulations size. We could also explore the laser intensity profile by running different simulations at different intensities, proportional to the focal cross section area.

Furthermore, better approximations were made for both single photon and collisional ionization by directly using experimental cross-sections. More importantly, we applied our ACI model that was developed at a different wavelength regime.

We first studied the influence of ACI on the maximum charge states seen for Xe_{80} clusters at 8×10^{12} W/cm^2 and Xe_{1000} clusters at 1.5×10^{13} W/cm^2. We have shown that the maximum charge state seen was increased by two states when ACI was enabled; from Xe^{3+} to Xe^{5+} for the smaller clusters and from Xe^{5+} to Xe^{7+} for the larger clusters. We did find that ACI had to be enabled for our simulations to be compatible with the 2002 DESY experiment, a clear indication that ACI plays an important role in the cluster dynamics.

Afterwards, we studied the charge state spectra shape as a function of cluster size at 8×10^{12} W/cm^2. For the shapes to be compatible with the experimental data, a spacial averaging of the intensity in the laser profile had to be performed. By allowing data from a lower intensity, both the maximum charge state (Xe^{4+}) and the most abundant one (Xe^{1+}) matched the experimental data for Xe_{90} clusters, but only when ACI was enabled. Due to computational limits, the largest cluster size simulated was $Xe_{5,083}$ (11 icosahedral shells), much smaller than the experiment' $Xe_{90,000}$ ($\sim$30 icosahedral shells), preventing any direct comparison.

The DESY experiment saw up to Xe^{8+} for the largest cluster size ($Xe_{90,000}$) which we could not simulate. It is not clear to us if the cluster size increase would show the increased charge states up to Xe^{8+}; four times the cluster size (from $Xe_{1,415}$ to $Xe_{5,083}$) just doubled the yield of Xe^{5+}. Does increasing by sixty times the cluster size able to increase not only the yield of Xe^{5+} but most importantly attain the Xe^{8+}? This is still an open question.

Finally, we looked at the potential depth influence on charge state spectra. Recombination to the ground state had to be enabled to prevent artificial electrons heating. A deeper potential cutoff allows stronger IBH through an augmented scattering angles, resulting in an increase of the maximum charge state seen as well as the most abundant one. This increase does saturates around 27.2 eV (1 Eh) when ACI is enabled, an effect that was not observed when ACI is not enabled.

Other groups studied the effect on the ionization spectrum of an atomic potential and found that it maximized energy absorption through IBH compared to a pure Coulombic potential shape. Such an atomic potential could be implemented in future work to validate the idea.

---

[1] H. Wabnitz, L. Bittner, A. R. B. de Castro, R. Dhrmann, P. Grtler, T. Laarmann, W. Laasch, J. Schulz, A. Swiderski, K. von Haeften, T. Mller, B. Faatz, A. Fateev, J. Feldhaus, C. Gerth, U. Hahn, E. Saldin, E. Schneidmiller, K. Sytchev, K. Tiedtke, R. Treusch, and M. Yurkov, Nature **420**, 4825 (2002).

[2] C. Jungreuthmayer, L. Ramunno, J. Zanghellini, and T. Brabec, Journal of Physics B: Atomic, Molecular and Optical Physics **38**, 30293036 (2005).

[3] C. Siedschlag and J.-M. Rost, Physical Review Letters **93**, 43402 (2004).

[4] U. Saalmann and J.-M. Rost, Physical Review Letters **91** (2003), 10.1103/PhysRevLett.91.223401.

[5] U. Saalmann, C. Siedschlag, and J.-M. Rost, Journal of Physics B: Atomic, Molecular and Optical Physics **39**, R39R77 (2006).

[6] I. Georgescu, U. Saalmann, and J.-M. Rost, Physical Review A **76**, 18 (2007).

[7] C. Greene and R. Santra, Physical Review Letters **91**, 14 (2003).

[8] R. Santra and C. Greene, Physical Review A **70** (2004), 10.1103/PhysRevA.70.053401.

[9] F. Herman and S. Skillman, *LANL* (Prentice-Hall, 1963).

[10] C. Bostedt, M. Adolph, E. Eremina, M. Hoener, D. Rupp, S. Schorb, H. Thomas, A. R. B. de Castro, and T. Mller, Journal of Physics B: Atomic, Molecular and Optical Physics **43**, 194011 (2010).

[11] E. Ackad, N. Bigaouette, K. Briggs, and L. Ramunno, Physical Review A **83**, 063201 (2011).

[12] E. Ackad, N. Bigaouette, and L. Ramunno, Journal of Physics B: Atomic, Molecular and Optical Physics **44**, 165102 (2011), arXiv:1011.5216.

[13] E. Ackad, N. Bigaouette, S. Mack, K. Popov, and L. Ramunno, New Journal of Physics **15**, 053047 (2013).

[14] J. E. Barnes and P. Hut, Nature **324**, 446449 (1986).

[15] P. Gibbon and G. Sutmann, in *Quantum Simulations of Complex Many-Body Systems: From Theory to Algorithms*, NIC Series, Vol. 10 (2002) p. 467506.

[16] J. B. West and J. Morton, Atomic Data and Nuclear Data Tables **22**, 103107 (1978).

[17] W. Lotz, Zeitschrift fur Physik **206**, 205211 (1967).

[18] H. Tawara and T. Kato, Atomic Data and Nuclear Data Tables **36**, 167353 (1987).

[19] A. Heidenreich, I. Last, and J. Jortner, The European Physical Journal D **35**, 567577 (2005).

[20] C. Bostedt, H. Thomas, M. Hoener, E. Eremina, T. Fen-

nel, K.-H. Meiwes-Broer, H. Wabnitz, M. Kuhlmann, E. Plonjes, K. Tiedtke, R. Treusch, J. Feldhaus, A. R. B. de Castro, and T. Moller, Physical Review Letters **100**, 133401 (2008).

[21] H. Thomas, C. Bostedt, M. Hoener, E. Eremina, H. Wabnitz, T. Laarmann, E. Plnjes, R. Treusch, A. R. B. de Castro, and T. Mller, Journal of Physics B: Atomic, Molecular and Optical Physics **42**, 134018 (2009).

[22] R. D. Cowan, *Nature*, Los Alamos Series in Basic and Applied Sciences, Vol. 140 (University of California Press, 1981) Chap. 8 and 16, p. 626627.

[23] M. Y. Amusia, *Atomic Photoeffect* (Springer, 1990).

[24] J. E. Barnes, Journal of Computational Physics **87** (1990), 10.1016/0021-9991(90)90232-P.

[25] C. Bostedt, H. Thomas, M. Hoener, T. Mller, U. Saalmann, I. Georgescu, C. Gnodtke, and J.-M. Rost, New Journal of Physics **12** (2010), 10.1088/1367-2630/12/8/083004.

[26] T. Fennel, K.-H. Meiwes-Broer, J. Tiggesbumker, P. M. Dinh, and E. Suraud, Reviews of Modern Physics **82**, 17931842 (2010).

[27] M. Hoener, C. Bostedt, H. Thomas, L. Landt, E. Eremina, H. Wabnitz, T. Laarmann, R. Treusch, A. R. B. de Castro, and T. Mller, Journal of Physics B: Atomic, Molecular and Optical Physics **41**, 181001 (2008).

[28] B. Iwan, J. Andreasson, M. Bergh, S. Schorb, H. Thomas, D. Rupp, T. Gorkhover, M. Adolph, T. Mller, C. Bostedt, J. Hajdu, and N. Tmneanu, Physical Review A **86** (2012), 10.1103/PhysRevA.86.033201.

[29] H. Iwayama, A. Sugishima, K. Nagaya, M. Yao, H. Fukuzawa, K. Motomura, X.-J. Liu, A. Yamada, C. Wang, K. Ueda, N. Saito, M. Nagasono, K. Tono, M. Yabashi, T. Ishikawa, H. Ohashi, H. Kimura, and T. Togashi, Journal of Physics B: Atomic, Molecular and Optical Physics **43**, 161001 (2010).

[30] M. Krikunova, M. Adolph, T. Gorkhover, D. Rupp, S. Schorb, C. Bostedt, S. Roling, B. Siemer, R. Mitzner, H. Zacharias, and T. Mller, Journal of Physics B: Atomic, Molecular and Optical Physics **45**, 105101 (2012).

[31] T. Laarmann, A. de Castro, P. Grtler, W. Laasch, J. Schulz, H. Wabnitz, and T. Mller, Physical Review Letters **92** (2004), 10.1103/PhysRevLett.92.143401.

[32] T. Laarmann, M. Rusek, H. Wabnitz, J. Schulz, A. de Castro, P. Grtler, W. Laasch, and T. Mller, Physical Review Letters **95** (2005), 10.1103/PhysRevLett.95.063402.

[33] R. Moshammer, Y. Jiang, L. Foucar, A. Rudenko, T. Ergler, C. Schrter, S. Ldemann, K. Zrost, D. Fischer, J. Titze, T. Jahnke, M. Schffler, T. Weber, R. Drner, T. Zouros, A. Dorn, T. Ferger, K. Khnel, S. Dsterer, R. Treusch, P. Radcliffe, E. Plnjes, and J. Ullrich, Physical Review Letters **98** (2007), 10.1103/PhysRevLett.98.203001.

[34] D. Rupp, M. Adolph, T. Gorkhover, S. Schorb, D. Wolter, R. Hartmann, N. Kimmel, C. Reich, T. Feigl, A. R. B. de Castro, R. Treusch, L. Strder, T. Mller, and C. Bostedt, New Journal of Physics **14**, 055016 (2012).

[35] U. Saalmann, Journal of Physics B: Atomic, Molecular and Optical Physics **43**, 194012 (2010).

[36] M. Schffler, K. Kreidi, D. Akoury, T. Jahnke, A. Staudte, N. Neumann, J. Titze, L. Schmidt, A. Czasch, O. Jagutzki, R. Costa Fraga, R. Grisenti, M. Smolarski, P. Ranitovic, C. Cocke, T. Osipov, H. Adaniya, S. Lee, J. Thompson, M. Prior, A. Belkacem, T. Weber, A. Landers, H. Schmidt-Bcking, and R. Drner, Physical Review A **78**, 013414 (2008).

[37] Z. B. Walters, R. Santra, and C. H. Greene, Physical Review A **74**, 43204 (2006), arXiv:0510187v3 [arXiv:physics].

[38] B. Ziaja, H. Wabnitz, F. Wang, E. Weckert, and T. Mller, Physical Review Letters **102** (2009), 10.1103/PhysRevLett.102.205002.

[39] B. Ziaja, H. Wabnitz, E. Weckert, and T. Mller, New Journal of Physics **10**, 043003 (2008).

[40] J. Zweiback, T. Ditmire, and M. Perry, Physical Review A **59**, R3166R3169 (1999).

[41] M. Arbeiter and T. Fennel, New Journal of Physics **13**, 053022 (2011).

[42] D. Bauer, Journal of Physics B: Atomic, Molecular and Optical Physics **37**, 30853101 (2004).

[43] C. Deiss, N. Rohringer, J. Burgdrfer, E. Lamour, C. Prigent, J.-P. Rozet, and D. Vernhet, Physical Review Letters **96** (2006), 10.1103/PhysRevLett.96.013203.

[44] F. Dorchies, T. Caillaud, F. Blasco, C. Bont, H. Jouin, S. Micheau, B. Pons, and J. Stevefelt, Physical Review E **71** (2005), 10.1103/PhysRevE.71.066410.

[45] R. von Pietrowski, K. von Haeften, T. Laarmann, T. Mller, L. Museur, and A. V. Kanaev, The European Physical Journal D **38**, 323336 (2006).

[46] A. Kramida, Y. Ralchenko, J. Reader, and N. A. Team, "NIST Atomic Spectra Database (ver. 5.0)," (2012).